6-21-2022

The Endurance Rocket Mission

Glyn Collinson
NASA Goddard Space Flight Center

Aroh Barjatya
Embry-Riddle Aeronautical University, barjatya@erau.edu

Robert Clayton
Embry-Riddle Aeronautical University, claytor8@erau.edu

Nathan Graves
Embry-Riddle Aeronautical University, gravesn@my.erau.edu

Henry Valentine
Embry-Riddle Aeronautical University, VALENTH1@my.erau.edu

See next page for additional authors

Space Science Reviews (2022) 218:39
https://doi.org/10.1007/s11214-022-00908-0

SPECIAL COMMUNICATION

The *Endurance* Rocket Mission

Gauging Earth's Ambipolar Electric Potential

Glyn Collinson · Alex Glocer · Rob Pfaff · Aroh Barjatya · Scott Bissett · Kolbjørn Blix et al. ***[full author details at the end of the article]***

Received: 6 January 2022 / Accepted: 18 May 2022

Abstract
NASA's *Endurance* sounding rocket (yard No. 47.001) will launch from Ny Ålesund, Svalbard in May 2022 on a solid fueled Oriole III-A launch vehicle. Its ∼ 19 minute flight will carry it to an altitude of ∼ 780 km above Earth's sunlit polar cap. Its objective is to make the first measurement of the weak "ambipolar" electric field generated by Earth's ionosphere. This field is thought to play a critical role in the upwelling and escape of ionospheric ions, and thus potentially in the evolution of Earth's atmosphere. The results will enable us to determine the importance to ion escape of this previously unmeasured fundamental property of our planet, which will aid in a better understanding of what makes Earth habitable. *Endurance* will carry six science instruments (with 16 sensors) that will measure the total electrical potential drop below the spacecraft, and the physical parameters required to understand the physics of what generates the ambipolar field. The mission will be supported by simultaneous observations of solar and geomagnetic activity.

Keywords Ambipolar · Electric fields · Ionosphere · Sounding rocket · Atmospheric escape · Endurance

Acronym List

ACS	Attitude Control System
CCMC	NASA Community Coordinated Modeling Center
DESA	Dual Electrostatic Analyzer
EISCAT	European Incoherent Scatter Scientific Association
ERU	Embry-Riddle Aeronautical University
ETU	Engineering Test Unit
GSFC	NASA Goddard Space Flight Center
IG	Ionization Gauge
MP	Megapixels
NASA	National Aeronautics and Space Administration

Note by the Editor: This is a Special Communication. In addition to invited review papers and topical collections, Space Science Reviews publishes unsolicited Special Communications. These are papers linked to an earlier topical volume/collection, report-type papers, or timely papers dealing with a strong space-science-technology combination (such papers summarize the science and technology of an instrument or mission in one paper).

Published online: 21 June 2022

NMS	Neutral Mass Spectrometer
NSROC	NASA Sounding Rocket Operations Contract
PANCAM	Panoramic Camera
PES	Photoelectron Spectrometer
REFIMS	Rotating Electric Field Ion Mass Spectrograph
SLP	Sweeping Langmuir Probe
SPDF	Space Physics Data Facility
SRPO	NASA Sounding Rockets Program Office
UNH	University of New Hampshire
WFF	NASA Wallops Flight Facility

1 Introduction

Discovering what processes govern atmospheric loss is important for understanding the evolutionary pathways of different planets and their ultimate potential for habitability. One mechanism thought to play a key role in the upwelling and outflow of ionospheric ions at any planet is a weak "ambipolar" (or "polarization") electric field generated by the topside of its ionosphere (Banks and Holzer 1968). At Mars, this field provides a substantial fraction of the energy required for oxygen ions to escape to space (Xu et al. 2018; Collinson et al. 2019). At Venus the field is so strong that it may have played a crucial role in the desiccation of the atmosphere (Collinson et al. 2016; Brecht and Ledvina 2021). However, at Earth, theory suggests that the ambipolar field is very weak (~ 0.4 V total potential drop Glocer et al. 2017), reducing the energy required for oxygen and nitrogen to escape. Nonetheless, while weak, Earth's ambipolar field is still thought to play an important role in driving the escape of ionospheric plasma which infuses ions into Earth's magnetosphere (Banks and Holzer 1968; Moore et al. 1997). This changes global magnetic reconnection rates (Shay and Swisdak 2004), inner magnetospheric plasma composition (Welling et al. 2011), and the distributions of plasmas throughout the magnetosphere (Glocer et al. 2009). Indeed, recent global simulations show that the contribution of ionospheric plasma to Earth's magnetosphere can be quite significant (Glocer et al. 2020). However, while important, this ambipolar electric field has yet to be successfully measured at Earth.

Endurance will be the first mission capable of resolving Earth's electric potential drop, determining its vertical structure, and investigating key underlying physics. *Endurance* will utilize a combination of in-situ sensors (to determine the potential drop and measure key contextual properties of the thermosphere and ionosphere), modeling (to probe deeper into the underlying physics than would be possible with observations alone), near-simultaneous observations from NASA's existing heliophysical observatories (for input into our models), and supportive ground-based measurements (for context and time history).

Endurance is scheduled for launch in May 2022. It will employ a technique successfully employed at Venus (Collinson et al. 2016) and Mars (Xu et al. 2018) to measure Earth's potential drop; involving measurement of photoelectrons escaping along open magnetic field lines from the dayside ionosphere. The need to launch onto open magnetic field lines necessitates a launch from the high latitude spaceport at Ny Ålesund (78.9°N geographic), in the Norwegian archipelago of Svalbard. The mission is named for the ship of exploration which Sir Ernest Shackleton and crew sailed to the Antarctic as part of the 1914–1917 Imperial Trans-Antarctic Expedition (Shackleton 1919). The mission logo can be seen in Fig. 1.

Key institutions involved in *Endurance* are listed in Table 1. The overall scientific lead institute is NASA's Goddard Space Flight Center, and the spacecraft and launch vehicle are

Fig. 1 *Endurance* mission logo

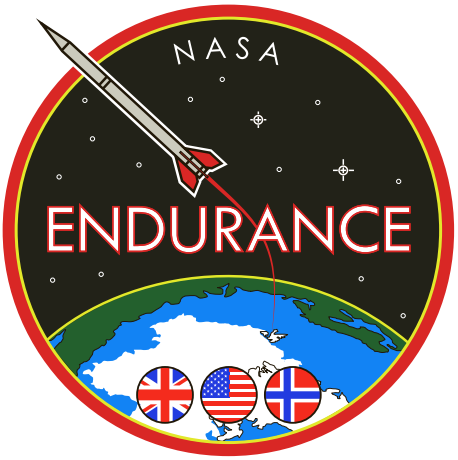

Table 1 *Endurance* institutional partners

Institution	Role in *Endurance*
NASA Goddard Space Flight Center, Greenbelt, MD, USA	Project management, two science instruments (Photoelectron Spectrometer, FIELDS package), science-team membership
NASA Wallops Flight Facility, Wallops Island, VA, USA	Mission management, spacecraft/launch vehicle design and fabrication, payload integration and testing, mission operations, field operations, one public outreach instrument
The Catholic University of America, Washington, DC, USA	P.I. institution
University of New Hampshire, Durham, NH, USA	Two science instruments (Ionization Gauges, Neutral Mass Spectrometer), science-team membership
Embry-Riddle Aeronautical University, Daytona Beach, FL, USA	One Science instrument (Swept Langmuir Probe), science-team membership
University of California at Berkeley, Space Sciences Laboratory, Berkeley, CA, USA	Data analysis software, science-team membership
University of Colorado at Boulder, Laboratory for Atmospheric and Space Physics, Boulder, CO, USA	Solar physics, science-team membership
University of Leicester, UK	RADAR Lead, science-team membership
Andøya Space, Norway	Launch range and field operations

being built at NASA's Wallops Flight Facility (yard No. 47.001 GE) by the NASA Sounding Rocket Program Office (SRPO) through the NASA Sounding Rocket Operations Contract (NSROC).

Endurance will launch on a three-stage Oriole III-A sounding rocket, each stage (Terrier-Oriole-Nihka) having extensive flight heritage, but not having flown before in this configuration. Nominal predicted apogee is 782 km, with splashdown 480 km downrange in the Greenland sea. During its $\sim$ 19 minute flight, its primary scientific instruments will measure: (1) the energy and flux of superthermal photoelectrons at an unprecedented resolution ($0.5\% \, \Delta E/E$); (2) the total electron density of the ionosphere; (3) spacecraft potential; (4) 2D electric fields and waves; (5) the density and composition of neutral gasses in the

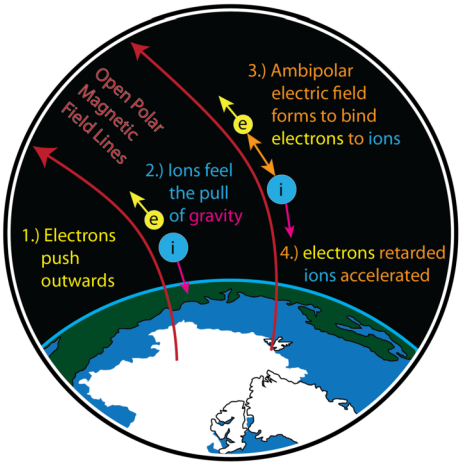

Fig. 2 Sketch showing the formation of the Earth's ambipolar electric field

thermosphere. Additionally, through two hosted payloads, *Endurance* will measure; (7) 3D magnetic fields; (8) color photographs of the view near apogee for public outreach.

This paper is laid out as follows. In Sect. 2, we describe the science background and objectives of *Endurance*. In Sect. 3 we describe the design of the mission; including an overview of the spacecraft, launch vehicle, the launch requirements, and the mission plan. In Sect. 4 we describe the scientific instruments carried by the *Endurance*. The paper is summarized in Sect. 5.

2 Science Background and Objectives

2.1 The Formation of Earth's Ambipolar Field

The ionosphere of any planet consists of ions and electrons in approximately equal numbers. In the absence of electrical forces, electrons, being three to four orders of magnitude lighter than ions, would easily escape the pull of gravity guided along the magnetic field, resulting in a net positive electric charge. However, the Coulomb force restricts electron motion away from the ions. As the electrons pull away, an electric field forms to resist their separation, preventing a net charge from forming and satisfying quasineutrality (see Fig. 2). This field acts equally (but oppositely) on both electrons and ions: restraining and slowing the negatively charged electrons, and pulling and accelerating positively charged ions out of the ionosphere. The associated ambipolar electric potential drop is critical to the formation of Earths "polar wind" which flows outward along open magnetic fields above our polar caps (Banks and Holzer 1968), and helps to transport ions to higher altitudes where other energization mechanisms may be at play (Moore and Khazanov 2010).

In order to understand what controls the strength of ambipolar field at any planet, we must consider the physics behind what is restraining the electrons as they "push" outwards (as in Fig. 2). Equation (1) (taken from Collinson et al. 2019) describes these processes, and the resulting generation of an ionospheric parallel ambipolar electric field ($E_{||}$)

$$E_{||} = -\frac{1}{en_e}\left[\underbrace{\frac{\partial P_e}{\partial s}}_{\mathbf{A.}} + \underbrace{\frac{\partial}{\partial s}\rho_e u_e^2 + \frac{B'}{B}\rho_e u_e^2}_{\mathbf{B.}} - \underbrace{\frac{\delta M_e}{\delta t}}_{\mathbf{C.}}\right] \tag{1}$$

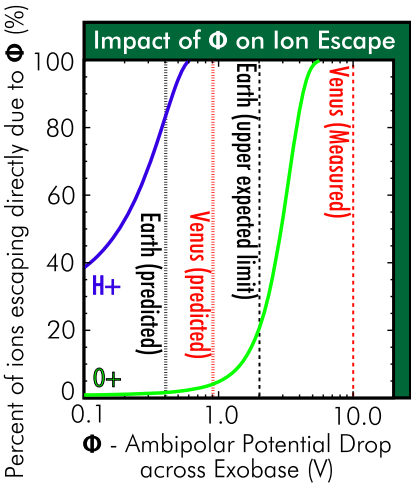

Fig. 3 Even a small change in ambipolar potential drop (Φ) significantly impacts ion outflow

This equation describes Ohm's law, as derived from the electron momentum equation assuming a scalar pressure. A full discussion of equation (1) can be found in Liemohn et al. (1997), Varney et al. (2014), or Collinson et al. (2019). In plain English, however, Equation (1) can be broken down into three basic physical processes; A.) Electron Pressure gradient; B.) Electron inertia; and C.) Collisional processes. At Earth, the dominant term in Equation (1) is often presumed to be term A.): The change in electron pressure (P_e) with distance (s) along the magnetic field line (Varney et al. 2014). The other two terms (B. and C.) involve the electron mass (m_e), which is very small when compared to the mass of the ions (m_i). Equation (1) may then be simplified to a form directly measurable by Langmuir Probe or from ground-based Radar:

$$E_{||} \approx -\frac{1}{en_e}\frac{\partial P_e}{\partial s} \tag{2}$$

While crucial to ion outflow, the ambipolar potential is extremely challenging to measure given its small magnitude. Current theory and simulations predict that it could be as weak as ≈ 0.4 V (calculated from our Polar Wind Outflow model, Glocer et al. 2007, 2009, 2012, 2017) across the exobase transition region (< 780 km). The first successful direct measurement of an ionospheric ambipolar potential drop was at the planet Venus (Collinson et al. 2016). Surprisingly, Venus' potential drop was found to be $+10$ V. Such a strong potential drop is an order of magnitude larger than the 0.9 V predicted by equation (2) (Collinson et al. 2019). This potential drop was found to be stable, persistent, and capable of accelerating oxygen ions directly to escape velocities. This surprising result raises a compelling question: *How strong is Earth's ambipolar potential?*

2.2 The Unknown Importance of Earth's Ambipolar Field in Mediating Ionospheric Escape

Figure 3 calculates the percentage of ions at the exobase (assuming a Maxwellian distribution) with sufficient energy to escape, for a given strength of Earth's ambipolar potential drop across the exobase (hereafter "Φ_{Earth}"). The figure demonstrates that even a small difference would have profound implications for the role that Φ_{Earth} plays in ionospheric outflow. The few previous attempts to measure Φ_{Earth} were case studies and only able to es-

timate an upper bound on the electric potential drop in Earth's ionosphere of ≤ 2 V (Coates et al. 1985; Fung and Hoffman 1991). If it is this strong, then no other mechanism is required for the escape of H^+, and it is directly responsible for the loss of $\approx 20\%$ of all O^+ ions. Indeed, even a small difference of ± 0.2 V relative to the expected value (0.4 V) would make an enormous difference to the fraction of H^+ directly escaping via this mechanism ($\approx 50\%$, 0.2 V vs 100%, 0.6 V, blue line, Fig. 3). If Φ_{Earth} were a Venus-like 10 V, then all O^+ ions would be accelerated to escape velocity.

Whilst such an extreme case is not expected at Earth, the vast disparity between theoretical predictions and observations at Venus challenges our fundamental understanding of ambipolar potentials, and strongly motivates the need for observations of the magnitude and altitude distribution of Φ_{Earth}. However, no mission has attempted to provide such observations.

2.3 Basic Concept: How to Measure Planetary Ambipolar Electric Potentials

Upon photoionization, atmospheric atoms emit electrons at discrete, constant, and well documented energies that are rigidly dictated by atomic physics. As these "photoelectrons" escape from Earth along the open field lines at the polar cap, they are decelerated by Earth's ambipolar field. During its quasi-vertical flight along open field lines in Earth's polar cap, *Endurance* will monitor how the energy spectra of photoelectrons evolve between 200 km $\rightarrow$ 780 km. Once these spectra have been corrected for the effects of e^- scattering and spacecraft potential, the electric potential drop below the spacecraft may be determined from the resulting shift in energy of these known spectral features.

Figure 4A shows an example of this technique being used to successfully measure the (10 V) ambipolar potential drop in the ionosphere of Venus (Collinson et al. 2016). These data were collected by the *Venus Express* ASPERA-4 Electron Spectrometer (ELS) (Barabash et al. 2007) at an altitude of approximately 600 km above Venus. A distinct feature of photoelectron energy spectra are sharp peaks in the 20–30 eV range from the ionization of neutral gas in the upper atmosphere by intense solar He-II 30.4 nm radiation (Nagy and Banks 1970). These "He-II photopeaks" have been observed throughout the solar system at Earth, Mars, Venus, and Titan (Coates et al. 2011). The precise energies of photopeaks vary at each world, depending on the composition of the neutral atmosphere. At Venus, the photopeaks observed by *Venus Express* are primarily produced by photoionization of O (not CO_2), resulting in strong photoemission of electrons at 22.29 eV and 23.69 eV (Coates et al. 2011). The ASPERA-4 ELS instrument had an energy resolution of 8% $\Delta E/E$ (Svedhem et al. 2007), and resolved this doublet as a single merged peak at 23 eV (Coates et al. 2008).

Between emission in the atmosphere and detection on a spacecraft, photoelectrons fall through two electric potential drops. The first is the planetary ambipolar potential drop (Φ_{Venus}, Φ_{Earth}), the second is the potential drop between the plasma and instrument arising from the electrical charging of the spacecraft (Φ_{SC}). For the example in Fig. 4A, the spacecraft was charged $\Phi_{SC} = +6$ V with respect to the ambient plasma. When the electron energy spectrum is corrected for the spacecraft potential drop, the ambipolar potential drop ($\Phi_{Venus} = 10.6$ V) can be directly measured from the shift from its formation energy (23 eV) to its measured energy (12.4 eV).

In order to employ this technique, a spacecraft must carry an electron spectrometer with sufficient energy resolution to resolve the energy shift in the photoelectrons resulting from the ambipolar potential (Φ_{Venus}, Φ_{Earth}). For the Venusian example in Fig. 4A, the 8% $\Delta E/E$ energy resolution corresponds to a resolution of 1.82 eV at 23 eV. Thus, with the ASPERA-ELS instrument, the smallest potential drop measurable was 1.82 V $= \pm 0.92$ V.

Figure 4B shows measurements of He-II photoelectron peaks at Earth (Doering et al. 1973; Su et al. 1998) by NASA's *Atmospheric Explorer E* spacecraft. At Earth, the predicted

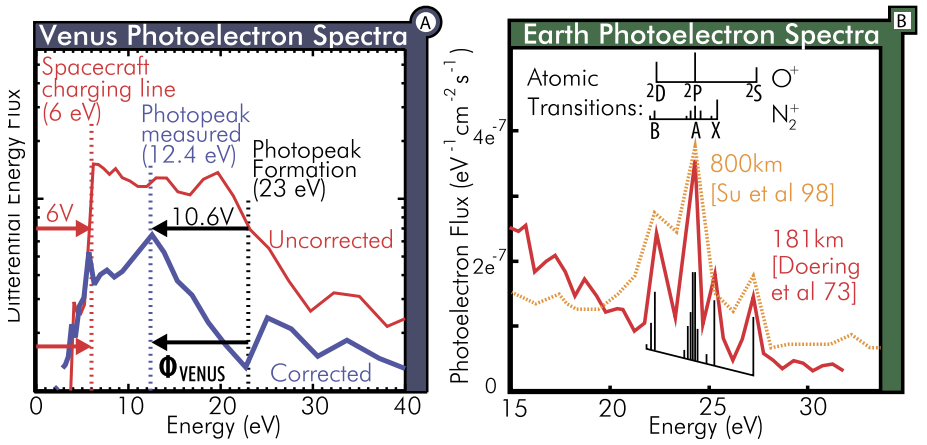

Fig. 4 Ionospheric photoelectrons can be used to measure the electric potential of a planet: Panel **A**.) Proof of concept: Venus' ambipolar potential drop successfully measured through a 10.6 eV shift in the He-II photopeak (Collinson et al. 2016); Panel **B**.) *Endurance* will measure Earth's photoelectrons at higher resolution than *Atmospheric Explorer E* (Doering et al. 1976; Su et al. 1998)

total potential drop is only 0.4 V (at 900 km altitude). Thus, to measure Earth's ambipolar potential drop (Φ_{Earth}), *Endurance* needs to resolve these photopeaks with a minimum resolution of at least 0.4 eV at 22 eV, or $\Delta E/E = 1.8\%$. As shown later in Sect. 4.1, the *Endurance* Photoelectron Spectrometer will far exceed this requirement with an energy resolution of 0.5% $\Delta E/E$. From past rocket experience, we anticipate that *Endurance* will charge to a potential of $\Phi_{SC} = +1\text{ V} \rightarrow +3\text{ V}$. As will be shown later in Sect. 4.2, this will be measured independently by a swept Langmuir probe.

2.4 Endurance Science Objective and Actions

The overriding science objective of *Endurance* is to determine the magnitude, nature, and vertical structure of Earth's ambipolar electric potential drop across the exobase transition and beyond. In order to address this objective, *Endurance* will perform three science actions.

A1: Determine the strength of the electric potential drop across Earth's exobase transition region (Φ_{Earth}) **on quiescent open field lines:** *Endurance* will carry an electron spectrometer with the highest energy resolution ever flown. This instrument, the Photoelectron Spectrometer (PES) will measure Φ_{Earth} by resolving the energy shift of known spectral features of electrons generated in the ionosphere (see Sect. 2.3). *Endurance* will make ~ 240 measurements of Φ_{Earth} to an accuracy between ± 0.17 V and ± 0.21 V (and better using peak fitting) over the ~ 15 minute flight. *Endurance* is thus instrumented to resolve even the weakest estimated total potential drop of $\Phi_{Earth} = +0.4$ V.

A2: Determine the vertical distribution of the electric potential: The vertical distribution of Φ_{Earth} is critical to understanding its impact on ionospheric upflow and outflow. *Endurance* will determine this vertical distribution through a combination of measurements and modelling: *Endurance* will fly as close to vertical as permissible (85° elevation) while aligned with open field lines across the exobase transition to a nominal altitude of ~ 808 km, continuously monitoring the potential drop below the spacecraft so that this vertical structure can be directly measured; *Endurance* will measure all parameters required to drive an accurate model of Φ_{Earth} and study its structure in more detail.

A3: De-tangle the competing underlying physical processes that drive the strength and distribution of the electric potential: The incoming solar flux ionizes the atmosphere, enhances the photoelectron and secondary electron populations, as well as heating and expanding the neutral thermosphere. It is the interplay of these effects which governs the generation and distribution of Φ_{Earth}. Separating out the relative contribution of each process is difficult to achieve using measurements alone. *Endurance* therefore will use a model of ion/electron transport and electric field formation on open field lines (The Polar Wind Outflow Model coupled with a photoelectron transport model GLOW), driven and constrained by observations to undertake a series of numerical experiments. Those experiments will unravel the intertwined contribution of these disparate processes to the observed potential structure.

3 Spacecraft and Mission Design

Endurance will achieve the above science objectives with a combination of *in-situ* rocket-borne measurements, ground based measurements, coordinated observations from NASA's existing Heliophysical observatories (Solar Dynamics Observatory (SDO), Solar Radiation and Climate Experiment (SORCE), Thermosphere, Ionosphere, Mesosphere, Energetics and Dynamics (TIMED) and modeling. The primary instrumentation will be flown on a sounding rocket, launched to a nominal apogee of 780 km. This high apogee is required to fly through the exobase transition region ($\approx$ 500 km).

As described previously in Sect. 1, one of the primary motivating factors to measure Earth's ambipolar field is to understand its role in the formation of the polar wind. While the ambipolar electric field is predicted to form everywhere on Earth, its strength and vertical structure may be different at the open field lines at poles (though it is important to note that it has yet to be been measured at any location on Earth). There are two factors that suggest this. Firstly, the ambipolar field is thought to be sensitive to the balance between plasma escaping from Earth's ionosphere and precipitating from above (Khazanov et al. 1997). The polar ionosphere is bombarded by a "polar rain" of soft electrons that precipitate down the open field lines from the solar wind (Winningham and Heikkila 1974). A second important difference between the polar ionosphere and the equatorial ionosphere is the orientation of the ambient magnetic field. It is thought that the ambipolar field at Earth is primarily driven by the electron pressure gradient along a field line (equation (2)). The vertical field lines near the pole will have a substantially steeper pressure gradient than the horizontal field lines near the equator, thus resulting in a very different electric potential.

These factors strongly motivate a launch along open magnetic field lines in Earth's polar cap. Thus, *Endurance* will be launched at a latitude of 78.93° North from Ny-Ålesund (on Svalbard, part of the Andøya Rocket Range (ARR)), on open polar magnetic field lines away from the cusp and auroral regions. *Endurance* will launch at the highest permissible elevation (85°), so that its two altitude profiles of Φ_{Earth} (upleg and downleg) are each confined to a magnetic flux tube 250 km across. *Endurance* will launch between 01:00 and 06:00 UT, May 2022 such that photoelectrons will be observed throughout the flight. An apogee of approximately 782 km is predicted for a trajectory that stays on open field lines and splashes down into the Greenland Sea north of Jan Mayen and off the coast of Greenland (Fig. 5A).

3.1 Endurance Instruments

Endurance will use the following rocket-borne instrumentation to measure the physical parameters which will be analyzed to provide closure on the science objectives:

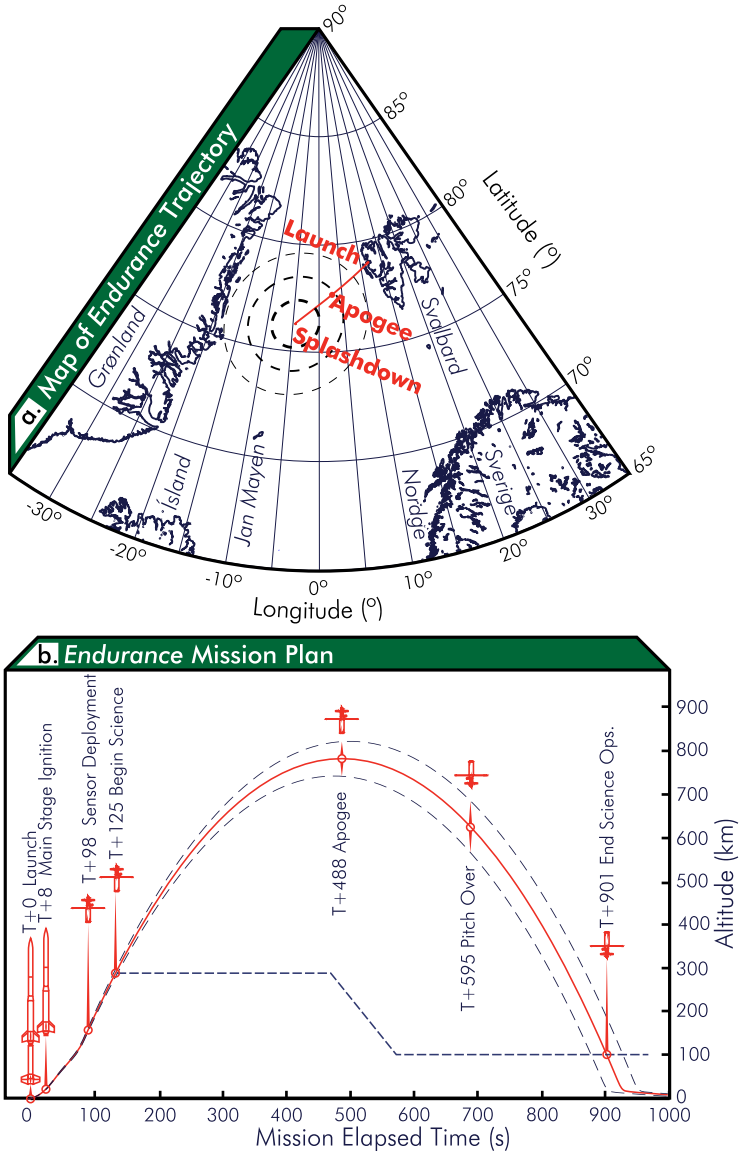

Fig. 5 **A**.) Map of the flight of Endurance over Earth's surface; **B**.) Schematic showing the trajectory of Endurance and major flight events

1. **Photoelectron Spectrometer** (PES) – Measures field-aligned inflowing and outflowing electron energy distributions from 10 eV to 1 keV.
2. **Sweeping Langmuir Probe** (SLP) – Measures the spacecraft floating potential (for correcting energy spectra, plasma density, and electron temperature).
3. **Electric Fields Instrument** (FIELDS) – Electric 2-axis DC fields and waves.
4. **Neutral Mass Spectrometer & Ionization Gauge** (NMS/IG) – Neutral densities by species (NMS) (160 km → 500 km), and total density using the simpler IG.

Table 2 *Endurance* instrument performance. Hosted payloads are marked with an asterisk (*)

Instrument	Institute	Parameter	Range	Accuracy	Cadence
Photoelectron Spectrometer (PES)	NASA GSFC	Superthermal Electrons	10 eV to 1 keV	0.5% $\Delta E/E$ or 16% $\Delta E/E$ (selectable)	10 s
Sweeping Langmuir Probe (SLP)	ERU	Thermal Plasma	1×10^3 cm^{-3} to 1×10^7 cm^{-3}	1×10^2 cm^{-3}	5 s
Electric Fields (FIELDS)	NASA GSFC	DC/AC Electric Fields	5 Hz to 20 kHz	20%	10 kHz
Neutral Mass Spectrometer (NMS)	UNH	Thermosphere Composition	1×10^6 cm^{-3} to 1×10^9 cm^{-3} 0 to 80 amu	20% cm^{-3} 1 amu	5 s
Ionization Gauge (IG)	UNH	Thermosphere Density	1×10^8 cm^{-3} to 1×10^{13} cm^{-3}	20%	5 s
Compass/ Magnetometer (MAG*)	NASA GSFC	DC/AC Magnetic Fields	$\pm$100 μT	2 nT	10 kHz
Panoramic Camera (PANCAM*)	NASA WFF	Color images for public outreach	N/A	N/A	240 s

In addition, *Endurance* will carry two hosted payloads that are not required for science closure.

5. **Magnetometer** (MAG) – Will act like a "ships compass" to later determine the bulk DC magnetic field orientation with respect to the payload.
6. **Panoramic Camera** (PANCAM) – A commercial off-the-shelf camera which will attempt to take a small number of color photographs near apogee for public outreach.

Table 2 summarizes their performance. Technical details and operating principles for each instrument are described in Sect. 4 (Instrument Descriptions). All instruments have flown successfully: SLP on the 2015 MTeX rocket (Triplett et al. 2018); FIELDS on the 2013 *VISIONS* rocket mission; and the neutrals package on the DYNAMO, DYNAMO-2, RENU-2, and Auroral Jet Rockets. A prototype sensor for the PES instrument has recently flown aboard the July 2021 DYNAMO-2 rocket mission.

3.2 Supporting Measurements

3.2.1 Solar EUV Spectral Irradiance

Endurance will be supported by measurements of solar EUV spectral irradiance by the Solar Dynamics Observatory (SDO), GOES-16, GOES-17, and GOES-18. These data will be used to provide a near-real time measurements of the solar spectrum, and in particular the He-II 304 Angstrom line responsible for generation of the He-II photopeaks that will be measured by the photoelectron spectrometer.

The EUV Variability Experiment on the Solar Dynamics Observatory (SDO-EVE) has a broad band photometer at 260–340 Angstroms with observations at 0.25 sec cadence.

SDO is at GEO orbit, so measurements are continuous. This particular band measurement is available with a 2–3 minute latency from EVE. The GOES-16, -17, and now -18 carry the EUV and X-Ray Irradiance Sensors (EXIS) instruments measure the He II 304 line with a passband of 10 Angstroms at 30-sec cadence. The GOES are also at GEO, and the data is available realtime (5-sec latency). While none of these instruments measure the full EUV spectral irradiance at high spectral resolution. None of these instruments measure the full EUV spectral irradiance at high spectral resolution. However, together they measure many discrete lines, bands, and emission features that are used in carefully calibrated and validated spectral irradiance proxy models so that the EUV spectrum from 0.1 to 195 nm can be re-constructed at 0.1 nm resolution from the SDO and GOES measurements. Hence, the solar spectral irradiance that is photoionizing the upper atmosphere will be available for the duration of the Endurance flight (in addition to the days leading up to the flight).

3.2.2 Ground-Based Radar

Endurance will be supported by ground-based measurements by the EISCAT Radar array. In the run-up to launch EISCAT Radar measurements of the electron temperature profile will be used to estimate the open/closed field line boundary, and thus ensure *Endurance* will be launching into open field lines. During the fight, EISCAT Radar will be used to measure electron and ion temperature, electron density, and ion velocity to complement the rocket measurements. These observations will be directly comparable to *in-situ* measurements of electron density and temperature by the Sweeping Langmuir Probe. The instantaneous vertical profiles of the ionosphere will be used to determine the electron pressure gradient on the field lines on which *Endurance* is flying, enabling a direct test of the current formation theory of Earth's ambipolar field (equation (2)).

3.3 Spacecraft Overview

Figure 6 shows the layout of *Endurance*. The launch vehicle is a three stage Oriole III-A solid fueled rocket (Terrier-Oriole-Nihka, Fig. 6a). In its launch configuration *Endurance* stands 14.2 m tall and weighs 255 kg. The payload consists of two elements; the service module containing the batteries, telemetry system, main computer, and attitude control system; and the exposed experiment module containing the scientific instruments. The exposed experiment module (Fig. 6b) is covered by a nosecone during launch, which is jettisoned prior to firing of the 3rd stage Nihka booster. At the very front of the spacecraft is the "Fo'c'sle", upon which is mounted the axial Ionization Gauge (IG) and Sweeping Langmuir Probe (SLP). The Photoelectron Spectrometer (PES) investigation consists of 8 Dual Electrostatic Analyzer (DESA) sensors mounted in pairs on short fold-down booms. Behind the Fo'c'sle is an exposed bay containing the rest of the neutrals package. The Neutral Mass Spectrometer (NMS) stows inside the neutral package bay for launch and hinges out after secondary engine cut-off. The radial ionization gauge (IG) looks out from a fixed position in the neutrals bay along the cross-track direction of travel.

At the bottom of the service module (Fig. 13) is the "Binnacle", a small deck that is exposed after jettison of the Nihka, upon which is mounted two hosted instruments; a low cost Panoramic Camera (PANCAM) for taking photographs for public outreach; and a fluxgate magnetometer that will measure the 3D vector of Earth's magnetic field.

3.4 Launch Requirements

In order to observe photoelectrons during the entire flight, the launch will be performed in May 2022 so that the flight occurs in daytime (despite the near-midnight launch window). It

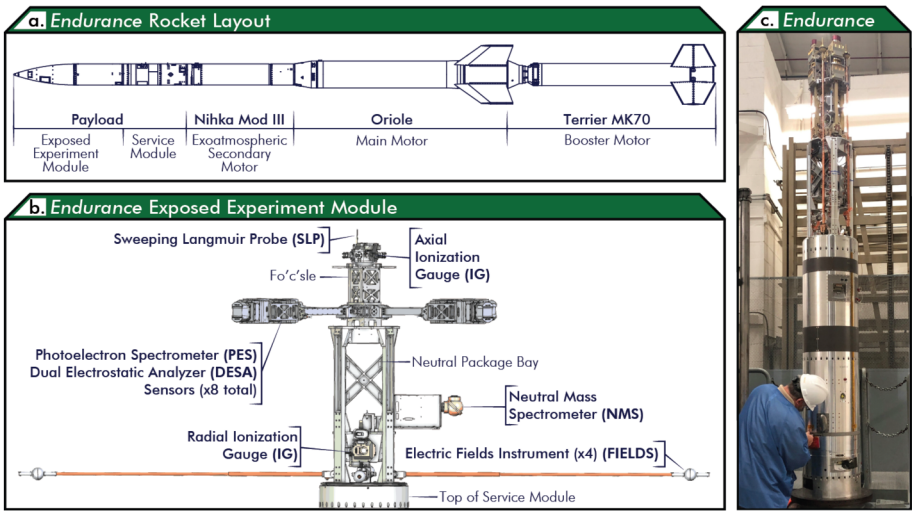

Fig. 6 **A**.) Layout of *Endurance* in launch configuration; **B**.) Drawing of exposed experiment module showing layout of the instrument package; **C**.) *Endurance* fully assembled and undergoing testing prior to shipment to the Arctic

is important that the thermosphere and ionosphere are minimally perturbed by geomagnetic activity, auroral activity is minimal, and the flight occurs away from field-aligned current regions (expected in the auroral regions and cusp, not open field lines). This is because our simulations predict that the heating of the thermosphere during geomagnetic activity increases the scale height, meaning that photoelectrons escaping from the ionosphere become more scattered. This results in a broadening of the photopeaks near apogee, which reduces our ability to precisely measure their energy shift.

The open-closed field line boundary will be studied prior to launch through examination of real-time data from the extensive ground-based magnetometer array and by global modeling from NASA's Community Coordinated Modeling Center (CCMC). In order to minimize the contribution of collisional degradation on the photopeaks we require: (1) low thermospheric densities are required to reduce photoelectron-neutral collisions; and (2) low ionospheric densities to reduce coulomb collisions with thermal electrons. We thus require a launch during low solar EUV (solar minimum-like) intensity to achieve these conditions, which we currently predict our 2022 launch window will provide. Live solar observations will thus be used to inform the launch decision, and ensure EUV is within acceptable parameters. Finally, *Endurance* will take advantage of the EISCAT RADAR at Svalbard to inform the locations of the cusp (to ensure its avoidance), and to provide supportive, real-time, ionospheric profiles during the flight.

3.5 Mission Plan

Table 3 shows an overview of the key events in the *Endurance* mission plan. *Endurance* will launch from Ny Ålesund between 1–6 UT. Its first stage, a Terrier Mk70 military surplus motor burns rapidly, accelerating *Endurance* to Mach 1.7 and lifting it up above the near-surface winds. The main stage, an Oriole sounding rocket solid motor, then burns for 29 seconds, accelerating *Endurance* to Mach 6.0. *Endurance* will then coast to the edge of the atmosphere (between 74 km and 79 km) and jettison the nosecone, revealing the exposed

Table 3 Mission timeline: NASA Rocket 47.001 *Endurance*

Mission elapsed time (s)	Nominal altitude (km)	Nominal range (km)	Event
0	0	0	Launch
6.2	1.7	0.2	Terrier Booster Burnout (BECO)
8.0	2.7	0.3	Oriole Main Engine Start (MES)
37.2	37.0	5.0	Oriole Burnout (MECO)
59.0	76.3	11.2	Nosecone Eject
66.5	88.8	13.3	Oriole Separation
67.5	90.5	13.6	Nihka Secondary Motor Start (SES)
72.9	100.0	15.3	Cross Kármán line into space
88.2	139.2	22.3	Nihka Burnout (SECO)
94.5	159.8	26.0	Payload/Nihka Separation
98.0	171.2	28.1	Boom and sensor deployment
104.0	190.3	31.6	ACS Align to magnetic field
125.0	254.8	43.8	Begin Science Operations
488.8	782.3	235.8	Nominal Apogee
595.0	738.6	289.6	Pitch over maneuver
901.4	100.0	456.4	End Science Operations
1123.0	0	479.7	Splashdown (Ballistic Impact)

experiment module (Fig. 6). With this mass jettisoned, the 3rd stage Nihka Mod III motor will fire for 20 seconds, accelerating *Endurance* to Mach 8.5.

Endurance will be spin-stabilized during launch and then three-axis stabilized during science operations to provide a steady platform for the 10 s integration of the PES instrument. After Nihka burnout, the steel cables securing the four electric field booms, four DESA booms, and the NMS are cut, hinging down under the centrifugal force of the spinning payload. *Endurance* will then use its attitude control system (ACS) to despin the payload and align its longitudinal axis to within $\pm 5^\circ$ of Earth's magnetic field. Nominal science operations will begin at 254 km on the upleg, and run through 100 km on the downleg. Apogee is predicted between 742 km (2σ low) and 822 km (2σ high), with a nominal altitude of 782.3 km. The spacecraft will pitch over prior to re-entry, when the spacecraft is above an altitude between 688.3 km and 788.2 km to realign the neutrals package with ram and collect data on the down-leg. The mission will come to an end with *Endurance* impacting the atmosphere at a velocity greater than Mach 14, sustaining heavy damage, and the wreckage then splashing down in the Greenland sea approximately 480 km away from the launch site.

4 Science Instruments and Simulated Data Products

4.1 Photoelectron Spectrometer (PES)

4.1.1 Overview of PES

The Photoelectron Spectrometer (PES) consists of 8 identical boom-mounted Dual Electrostatic Analyzer (DESA) sensors (Fig. 7c) and a main electronics control box (Fig. 7d). PES

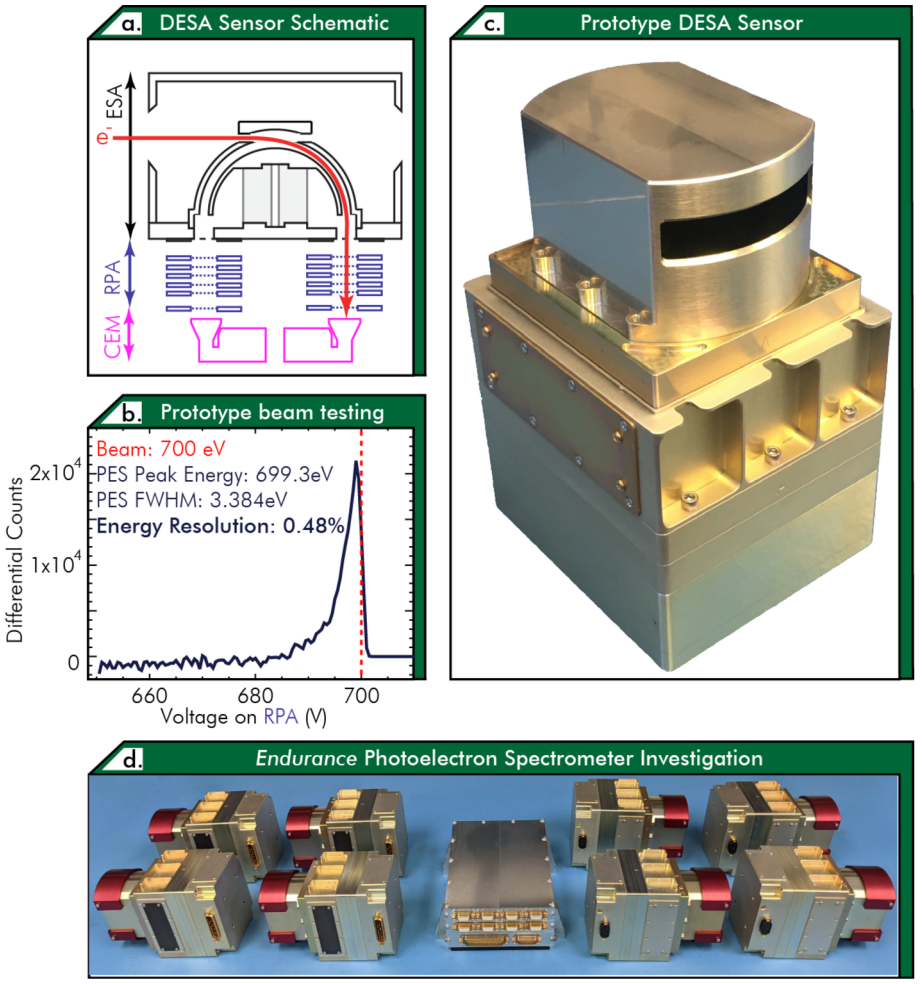

Fig. 7 **a**.) Schematic of a Dual Electrostatic Analyzer (DESA) sensor, eight of which will fly aboard the *Endurance* as part of the Photoelectron Spectrometer (PES) investigation; **b**.) Laboratory data from electron beam testing of the Engineering Test Unit DESA sensor (serial No. DESA-NX-02) demonstrate it has the required energy resolution (0.5%); **c**.) Photograph of the DESA Engineering Test Unit ETU; **d**.) Photograph of the *Endurance* Photoelectron Spectrometer investigation

will simultaneously measure (1) superthermal electrons (10 eV–1 keV) inflowing and outflowing from Earth's ionosphere at a standard energy resolution of $(\Delta E/E)$ 16% (Fig. 8c) and (2) Outflowing photoelectrons (20–28 eV) with a high energy resolution $(\Delta E/E)$ of 0.5% (Fig. 8c).

PES has a total geometric factor of 1.8×10^{-3} cm^{-2} sr^{-1} eV/eV from all 8 DESA sensors. PES has two look directions, one upward (field-aligned), the other downward (field-aligned $+180°$). Each sensor has a $8° \times 10°$ fixed field of view (FOV). Note only field-aligned components are required for science closure, not full pitch-angle distributions, and the DESA sensors will be physically aligned to within $\pm 5°$ of the magnetic field (Fig. 6).

The DESA sensors achieve their high energy resolution through a combination of two common types of plasma analyzer (Collinson et al. 2018). Electrons entering PES (Fig. 7a) first traverse a "Top Hat" electrostatic analyzer (ESA) (Carlson et al. 1982). The ESA provides an initial broad bandpass energy filter to incoming electrons. Electrons then pass through a high-resolution Retarding Potential Analyzer (RPA Enloe 1994), which may be electrically biased such that only electrons above a set threshold energy may reach the detector. Electrons are detected by a pair of Channel Electron Multipliers (CEM). The ESA scans over the full energy range (10 eV–1 keV) in logarithmic steps. At each step around photopeak energies (20–28 eV) the RPA scans across the ESA's output in 0.1 eV steps. An abrupt change in counts as the RPA scans over each photopeak reveals their precise energy (as demonstrated shortly). *Endurance* is expected to charge to around $+1$ V $\rightarrow +3$ V with respect to the plasma, resulting in a -1 eV $\rightarrow -3$ eV shift in the photopeaks. The energy range of the high-resolution scanning has been chosen to still observe at least one photopeak even in the case of the most extreme ($+3$ V) spacecraft potential expected.

Outside of photopeak energies, the ESA alone is used to rapidly measure the flux of precipitating particles (16% $\Delta E/E$ with ESA alone vs 0.5% $\Delta E/E$ for ESA+RPA). PES makes one complete energy sweep (200 ESA/RPA voltages) in 10 s.

Figure 7b shows laboratory data from the Engineering Test Unit DESA sensor (Fig. 7c), demonstrating that the DESA sensor can resolve photopeak-like structures at the 0.5% energy resolution ($\Delta E/E$) required for *Endurance*. A monoenergetic beam of electrons (simulating a photopeak) was fired into the prototype over the entire energy/angle acceptance bandpass of the instrument, with the voltage on the ESA kept steady. As the RPA scans across the energy of the beam, the counts detected sharply changes. Differentiating these data produces an energy spectra (Fig. 7b), showing a sharp peak at the precise energy of the beam with 0.5% full-width at half-maximum ($\Delta E/E$). This energy resolution was constant at all energies tested.

4.1.2 Predicted Results of the *Endurance* Photoelectron Spectrometer

Each scan of PES (10 eV to 1 keV) will take 10 seconds, the majority of which is spent scanning for photopeaks between 20 eV and 28 eV. Figure 8A shows a prediction of how the nominal altitude of *Endurance* will vary with flight time. Using this flight model, the altitude was calculated for each 10 second integration of PES. The energy spectrum of superthermal electrons was then calculated for each of these altitudes using the GLOW model which has been coupled to the Polar Wind Outflow Model (PWOM) (Solomon and Abreu 1989; Glocer et al. 2007, 2009, 2012, 2017, 2018). These spectra were then processed through the Photoelectron Spectrometer instrument model, which converts the flux into counts and adds Poisson noise to create a simulated data product.

Figure 8b–e shows simulated Photoelectron Spectrometer data from the instrument model. Figure 8b shows a time-energy spectogram for the whole flight of the standard resolution data product (10 eV to 1 keV at 16% energy resolution) measured using the electrostatic analyzer (ESA) alone. Figure 8c shows a time-energy spectrogram of the high resolution data product (20 eV to 28 eV at 0.5% energy resolution) from the combined ESA and retarding potential analyzer (RPA). This model predicts that three photopeaks will be resolved throughout the flight. Note that this calculation does not include the shift due to Earth's ambipolar electric field, and the decrease in energy apparent in Fig. 8c is from electrons colliding with the neutral atmosphere as they escape upwards along the field lines.

Figure 8d shows what this model predicts PES will observe immediately after switching on at ~ 250 km. Simulated superthermal electron spectrum is shown in green. The PES

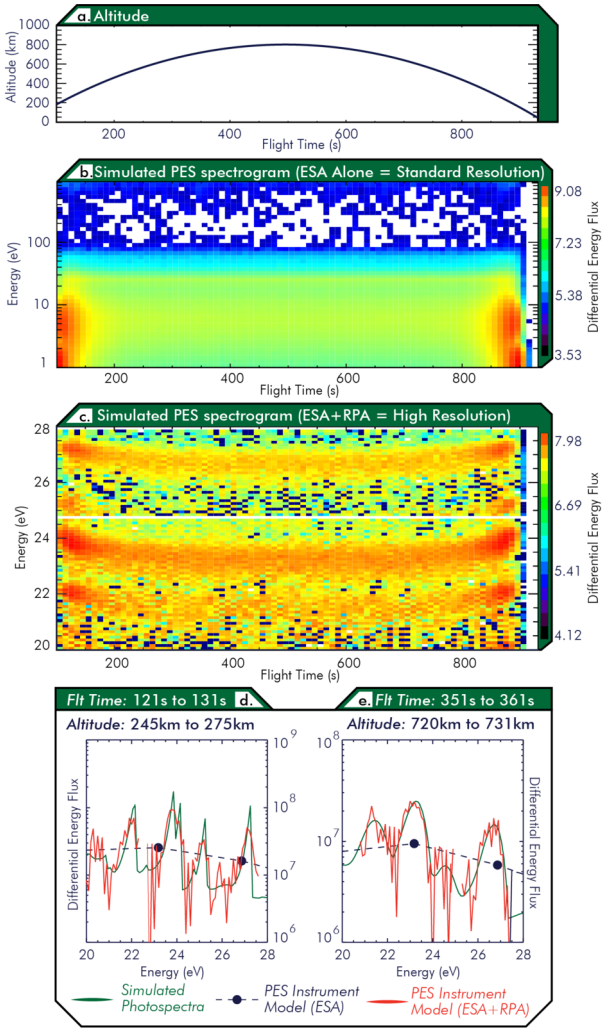

Fig. 8 **a**.) Predicted altitude of the *Endurance* as a function of flight time; **b**.) Simulated Time/Energy spectrogram from the *Endurance* Photoelectron Spectrometer (ESA Alone); **c**.) Simulated high resolution time/energy spectrogram from *Endurance* PES; **d**.) Simulated electron energy spectrum from just after the PES instrument is enabled at ∼ 250 km showing four distinct photopeaks; **e**.) Simulated electron energy spectrum from above Earth's exobase, showing the spreading of the photopeaks from collisions with the atmosphere

instrument model predicts that the high resolution data product (ESA+RPA, red) will resolve four photopeaks between 20 eV and 28 eV. The PES instrument model also predicts that the standard resolution data product (ESA alone, blue) will measure the general energy flux around these energies, but will not resolve the photopeaks.

Figure 8e shows another predicted electron energy spectrum, this time from above the exobase on ascent towards apogee. This plot shows the expected broadening of the peaks due to collisions between the electrons and the neutral atmosphere.

4.2 Sweeping Langmuir Probe (SLP)

Mounted on the Fo'c'sle at the very front of *Endurance*, is the Sweeping Langmuir Probe (SLP). The SLP needle probe (Fig. 9) is mounted forward so that it is the first part of the spacecraft to encounter undisturbed plasma. SLP will provide absolute plasma density, electron temperature, as well as the potential difference between the spacecraft and the ambient

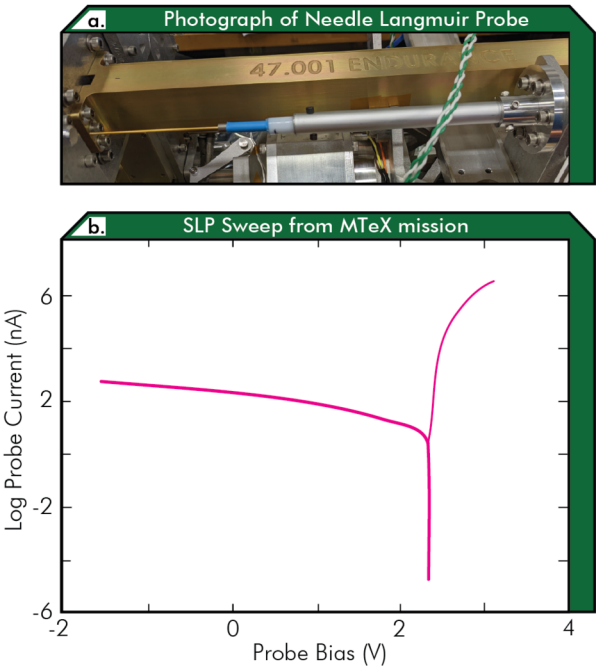

Fig. 9 **a**.) *Endurance* SLP needle probe (payload booms stowed); **b**.) SLP sweep from MTeX mission (85 km)

plasma. SLP will perform an active (20 ms) sweep once every 5 seconds, at which time PES will pause integration so that there is no interference with PES measurements. SLP is derived from that flown on the 2015 MTeX rocket (Fig. 9).

SLP is a traditional Langmuir Probe wherein a sweeping voltage (±5 V) is applied to a gold plated cylinder (5 cm long and 1 mm diameter). The sensor has guards on one side (operated at the same potential), separated from the sensor by 1 mm. The area of the probe is small with respect to the spacecraft (ratio of a few thousands), which will avoid payload floating potential swings as the SLP is swept (Szuszczewicz 1972). Each of the observed I-V curves from the SLP will be reduced to electron temperature, ion and electron density and the spacecraft charging/floating potential. A fast sweep rate will be used to reduce the effect of surface contamination (Oyama et al. 2012). Figure 9b shows two consecutive in-flight sweeps from a non-heated SLP that was swept at 10 Hz. No hysteresis is seen and electron temperature can be derived cleanly.

4.3 Electromagnetic Fields and Waves Package (FIELDS)

The purpose of the FIELDS instrument is to characterize the electrodynamics of the ambient plasma including the presence of plasma waves and irregularities which might affect the measured electrons. FIELDS will measured the large scale DC/AC electric fields using the standard "double probe" technique: Four spherical sensors with embedded pre amps will be extended to form an orthogonal 2-axis, 3 m (tip-to-tip) double probe in the plane perpendicular to the rocket axis. The double probes will capture both electrostatic and electromagnetic modes up to frequencies of 5 MHz.

Measurements of the phase difference between the two orthogonal receivers will help establish the electrostatic/electromagnetic nature of any ELF/VLF plasma wave modes encountered in the polar cap. The wave receiver also includes an HF channel to observe the

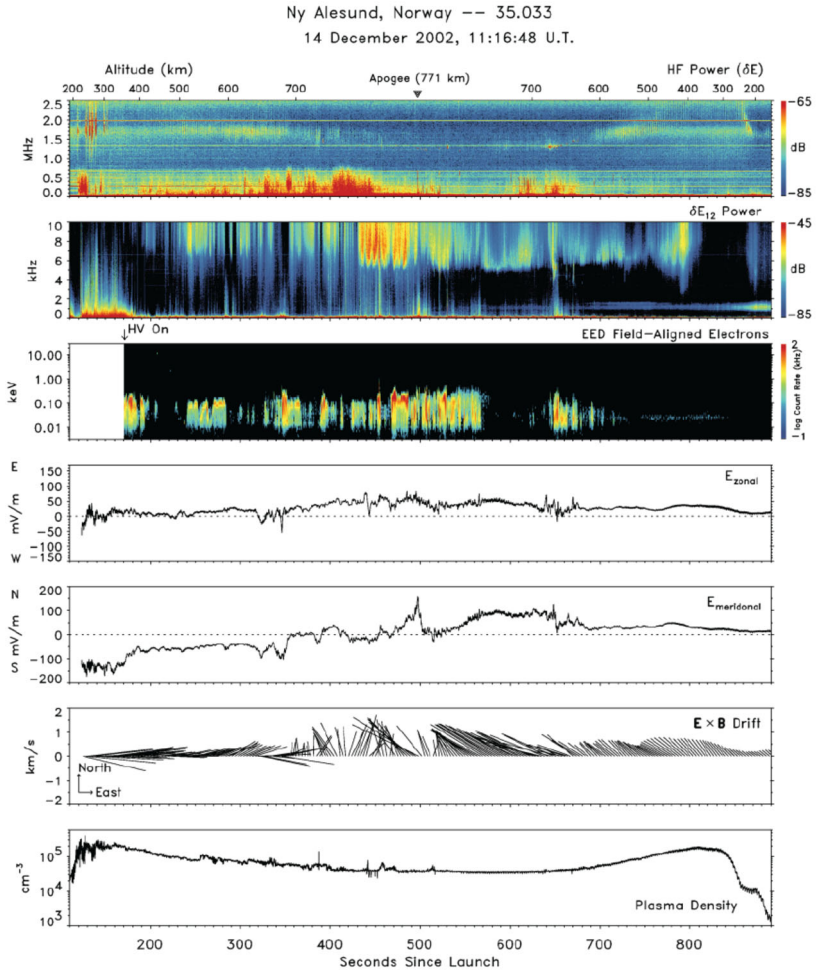

Fig. 10 Electric waves and ambient DC magnetospheric electric fields measured in the cusp above Ny-Ålesund from the FIELDS instrument from NASA Sounding Rocket 35.033 (Pfaff et al. 2003)

presence of any waves near the electron plasma frequency, such as HF Langmuir waves. The electronics will return FFT power spectra and "snapshots" of the HF data at regular intervals. In some cases, cutoffs observed at the plasma frequency can be used to calibrate the densities obtained from the Langmuir probe. The detector will also provide 2-axis DC electric fields using the assumption that $E.B = 0$, or that there are no parallel electric fields.

Figure 10 shows FIELDS measurements from a rocket in the cusp above Ny-Ålesund (Pfaff et al. 2003) from NASA Sounding Rocket 35.033 (771 km apogee), showing sonograms of HF and VLF waves as well as the ambient DC electric fields of magnetospheric origin. The wave receiver on *Endurance* will gather measurements of any similar such waves and plasma structures, should they exist along the rocket trajectory. This measurement of the ambient magnetospheric electric fields will help characterize the plasma environment from which the much smaller ambipolar electric fields will be ascertained using our sensitive electron instrument.

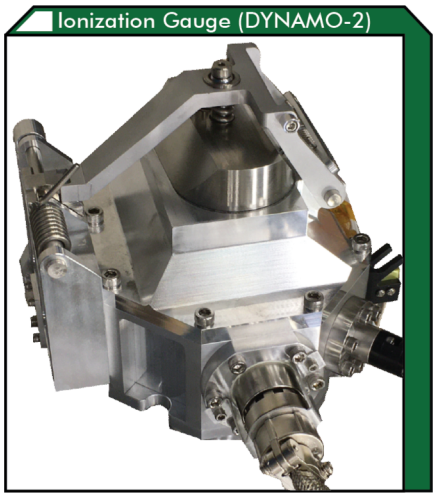

Fig. 11 Ionization Gauge from the 2021 DYNAMO-2 Rocket, identical to that which will be flown aboard *Endurance*

4.4 Neutral Gas Ionization Gauge (IG)

The Ionization Gauge (IG) is included in the payload to provide measurements of total atmospheric density and its variation, as well as the temperature profile. The measurement objective for the IGs on *Endurance* is to provide profiles of temperature and density in support of determination of the atmospheric structure during the flight. Two sensors will be used to provide sampling of the flow conditions around the payloads, one viewing the forward "ram" direction and one viewing transverse to the spin axis. Bayard-Alpert ionization gauges are employed as the sensors. The principle of operation is that a volume of the gas to be measured is partially ionized by a stream of electrons, then the resulting ions are collected by an electrode. The density of the gas is proportional to the ratio of the electron current to the collected ion current.

The IG utilizes two sensors to sample two angles of attack, one on the forward Fo'c'sle deck and one oriented radially from the payload (Fig. 6b). This geometry is similar to that used for several previous missions, including the RENU-2 mission of December 2015 and the Dynamo missions of July 2011 and July 2013. The payload will be oriented by its ACS throughout the flight so that the radially mounted sensor will face along the direction of travel over Earth's surface. The IG utilizes miniature gauges available from Anelva Corporation. The sensor is depicted with its thermalization chamber and vacuum door in Fig. 11. The cap is sealed before launch and opened at altitude. Electronics control and measure the emitted electron current as well as measure the collected ion current. High-resolution, high-speed analog-to-digital converters provide rapid (1 kHz) measurements spanning a large dynamic range ($\sim 10^6$) in pressure.

4.5 Neutral Mass Spectrometer (NMS)

4.5.1 NMS Overview

The Neutral Mass Spectrometer (NMS) is inherently an ion mass spectrograph fed by ions created from the neutral gas to be measured. The NMS combines an ionizer based on the IG

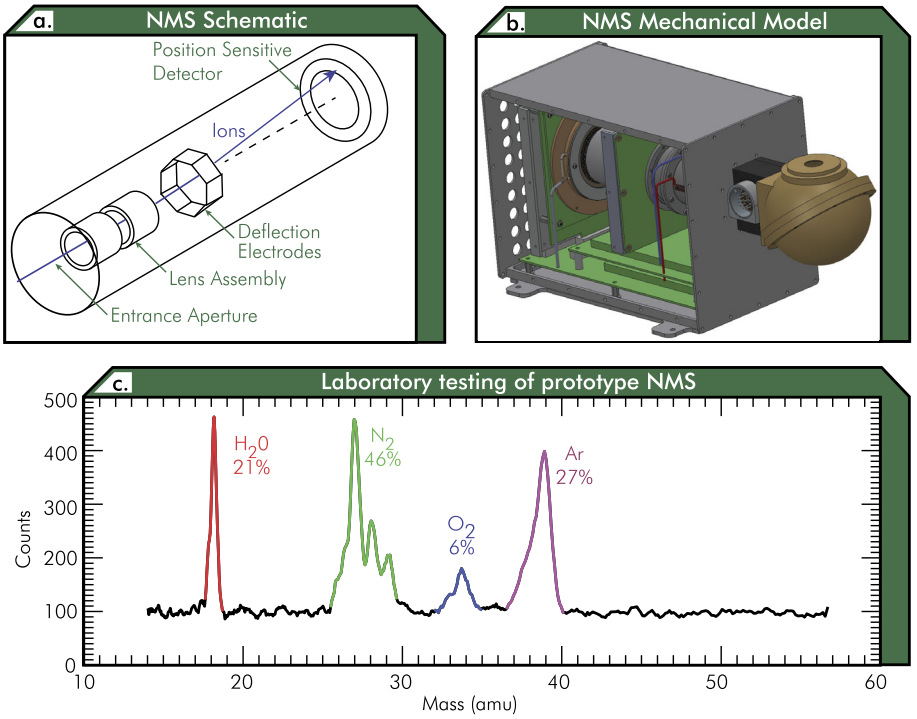

Fig. 12 **a**.) Schematic of REFIMS sensor; **b**.) Rendering of the NMS with side panel removed to show internal structure; **c**.) Block diagram of the NMS; **d**.) Data from laboratory tests of the prototype NMS

de-scribed above with a Rotating Electric Field Ion Mass Spectrograph (REFIMS) (Clemmons and Herrero 1998). REFIMS utilizes a time-dependent electric field and incorporates a position-sensitive microchannel plate (MCP) detector.

Figure 12a contains a schematic diagram of the sensor. Cold ions are admitted at the aperture, then accelerated and focused by the focusing electrodes. The time dependent field is produced by the deflection electrodes as a field directed perpendicular to the device axis which "rotates" around the axis in time. Ions are then dispersed in a time dependent manner such that the image formed on the position-sensitive detector yields mass in formation by "de-spinning" the image. The sensor is faster than other techniques because all masses are imaged simultaneously, obviating the need for time-consuming mass scanning. The cold ions are made by ionizing the neutral gas with an ionizer.

4.5.2 NMS Description

Rammed gas to be measured is admitted into an accommodation chamber similar to that used in the IG. The ionizer is attached to the chamber and ionizes accommodated gas and feeds the resulting ions to the REFIMS analyzer. The ionizer circuitry is based on the filament and control circuitry used in the IG instrumentation. The analyzer is about 150 mm in length and 50 mm in diameter. The deflection field employs sinusoidal signals of about 250 kHz at 70 V amplitude. The imaging detector consists of a chevron pair of 50 mm MCPs followed by a ring of small, equally spaced anodes. Each ion that impinges on the

MCP chevron in front of an anode produces a charge pulse which is then amplified by a charge amplifier. Each pulse then causes the increment of an appropriate channel in the spectrum accumulation electronics. The appropriate channel is determined from the position of the anode sending the pulse and the phase of the deflection field at the time of detection (effecting the "de-spinning" mentioned above).

4.5.3 NMS Predicted Performance

The NMS covers all of the main thermospheric species that will be encountered by *Endurance* (He, O, N_2, O_2) with resolution better than 1 amu by accumulating a 512-point mass spectrum over the mass range 0–80 amu every 4 ms. The spectral resolution is proportional to the square root of mass, and the parameters chosen for the flight instrument yield resolution better than 1 amu at mass number 64 and about 0.1 amu at mass number 1.

Vacuum chamber testing produced the mass spectrum seen in Fig. 12d. The expected major species are evident, and the spectrum compared well with simultaneous readings from a commercial residual gas analyzer. This test demonstrated the overall feasibility of the NMS concept.

4.6 Magnetometer (MAG) – Hosted Payload 1

Endurance is giving a free ride to space for two hosted guest instruments. The first is magnetometer (MAG) which will measure DC and AC magnetic fields. The longitudinal axis of *Endurance* needs to be aligned to within $\pm 5^\circ$ of Earth's magnetic field during science operation. This requirement is sloppy enough that this alignment will be achieved in-flight by pointing the spacecraft according to pre-programmed global magnetic field model. After the flight, bulk DC magnetic field measurements from MAG will be used to verify the actual in-flight alignment with respect to the ambient magnetic field encountered. Thus, MAG will effectively act as *Endurance's* "ship's compass".

MAG combines a commercial Billingsley 3-axis fluxgate with a high-precision A/D converter built by NASA Goddard Space Flight Center. The magnetic field data are digitized (simultaneously with the electric field data) to 18-bit precision. The sensor includes a frequency response that extends to several 100 Hz. Each component is sampled at 2 kHz providing high time resolution. Since MAG is a hosted payload and not required for science closure, it was included on a "do no harm" basis. Thus, MAG is mounted on the aft body of the payload (in a region called the "Binnacle", see Fig. 13), and not on its own deployable boom which would add complexity and mass. While no magnetic cleanliness requirements were levied upon *Endurance*, MAG has been calibrated using the Wallops magnetic facility and is expected to successfully measure at least the bulk direction of DC vector fields.

4.7 Panoramic Camera (PANCAM) – Hosted Payload 2

Endurance will carry a color panoramic camera (PANCAM) for the purposes of taking photographs for public outreach. PANCAM is a low-cost instrument that is bought commercially off-the-shelf. Earth's limb will be imaged at 12 Megapixel (MP) resolution using a commercial Raspberry Pi High Quality Camera, and the data processing and commanding handled by a Raspberry Pi Zero single-board computer. PANCAM is mounted on the aft binnacle of *Endurance* (see Fig. 13). Development of PANCAM, and its integration with the *Endurance* telemetry system was performed at NASA Wallops Flight Facility.

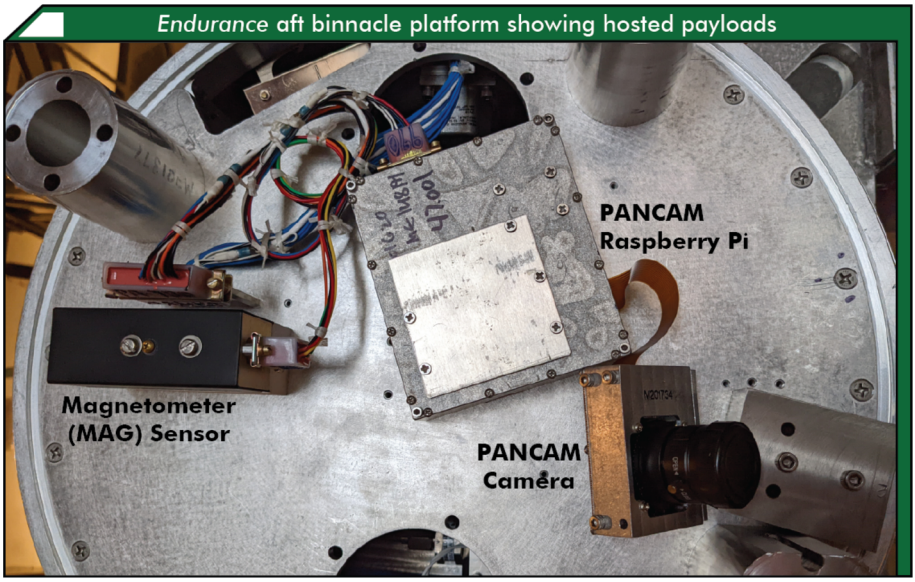

Fig. 13 Photograph showing the aft binnacle of *Endurance*, home to two hosted payloads

During the flight, the *Endurance* spacecraft will send a series of timed commands to PANCAM which trigger it to take a photograph. The number of photographs is heavily limited by the asynchronous serial bus down which images are transmitted to the encoder, and as a result PANCAM will only be able to take 5 images during the flight. Four of these images will be downsampled to lower resolution. All images will be transmitted as a .jpg file to the *Endurance* telemetry encoder for downlink to Earth. The first two images ($\sim$ 160 km and $\sim$ 326 km) will be reduced to 1 MP thumbnails. The third photograph ($\sim$ 487 km) will be downsampled to 8 MP. The fourth photograph will be taken near apogee ($\sim$ 778 km) and downlinked at full 12 MP resolution. The fifth photograph ($\sim$ 412 km) will be taken after the pitch-over maneuver on the downleg. All photographs will be framed and planned in advance, since the attitude of the spacecraft and hence the pointing of PANCAM throughout the flight are known. Figure 14 shows a simulated image from PANCAM taken at 800 km. This image was created in Google Earth Engine, using the nominal trajectory of *Endurance* and planned pointing of PANCAM.

5 Summary

The *Endurance* rocketship (yard No. 47.001) is scheduled to launch in May 2022 from Ny Ålesund, Svalbard. *Endurance* will voyage to an altitude of $\sim$ 780 km above Earth's sunlit polar cap on a mission to attempt to make the first measurement of the weak "ambipolar" electric field generated by the ionosphere.

Endurance will carry six science instruments (with 14 sensors). The Photoelectron Spectrometer (PES), consisting of 8 Dual Electrostatic Analyzer (DESA) sensors and a main electronics box will measure the total potential drop below the spacecraft. The Sweeping Langmuir Probe (SLP) will make active sounding of the potential difference between the spacecraft and plasma, plus characterizing the density and temperature of ionospheric plas-

Fig. 14 Simulated image from Endurance PANCAM near 800 km (Google Earth Engine)

mas. The 2 Ionization Gauges (IG) will measure the density of the neutral thermosphere, and the Neutral Mass Spectrometer (NMS) will determine the composition of the thermosphere. The Electric Fields instrument (FIELDS) will use its 4 electric field booms to monitor for wave activity which may perturb the ambient electron population, and passively monitor the relative change in spacecraft potential between active sweeps of the SLP. Finally, the Panoramic Camera (PANCAM) will attempt to take color images for public outreach. The mission will be supported by EISCAT observations, and simultaneous observations of solar and geomagnetic activity. Science closure will be achieved through a combination of data analysis and theory and modeling with the Polar Wind Outflow Model (PWOM).

Endurance is a collaboration between three nations. The United States of America is building and flying the rocketship. The Kingdom of Norway owns and operates the launch site as part of the Andøya Rocket Range. The United Kingdom of Great Britain and Northern Ireland is providing RADAR support through its contribution to the EISCAT program. All data will be made publicly available after the mission through NASA's Space Physics Data Facility (SPDF). Any researchers potentially interested in *Endurance* data are encouraged to reach out to the principal investigator (electronic address at time of writing: glyn.a.collinson@nasa.gov).

Acknowledgements The *Endurance* Rocket Mission is funded through NASA's Heliophysics Technology and Instrument Development for Science (HTIDS) program (grant No. 80NSSC19K1206) and NASA's Sounding Rocket program. RADAR support for *Endurance* is funded through the United Kingdom's contribution to the European Incoherent Scatter (EISCAT) Scientific Association.

References

P.M. Banks, T.E. Holzer, J. Geophys. Res. **73**, 6846 (1968). https://doi.org/10.1029/JA073i021p06846

S. Barabash, J.A. Sauvaud, H. Gunell, H. Andersson, A. Grigoriev, K. Brinkfeldt, M. Holmström, R. Lundin, M. Yamauchi, K. Asamura, W. Baumjohann, T.L. Zhang, A.J. Coates, D.R. Linder, D.O. Kataria, C.C. Curtis, K.C. Hsieh, B.R. Sandel, A. Fedorov, C. Mazelle, J.J. Thocaven, M. Grande, H.E.J. Koskinen, E. Kallio, T. Säles, P. Riihela, J. Kozyra, N. Krupp, J. Woch, J. Luhmann, S. McKenna-Lawlor, S. Orsini, R. Cerulli-Irelli, M. Mura, M. Milillo, M. Maggi, E. Roelof, P. Brandt, C.T. Russell, K. Szego, J.D. Winningham, R.A. Frahm, J. Scherrer, J.R. Sharber, P. Wurz, P. Bochsler, Planet. Space Sci. **55**, 1772 (2007)

S.H. Brecht, S.A. Ledvina, J. Geophys. Res. Space Phys. **126**(2), e27779 (2021). https://doi.org/10.1029/2020JA027779

C.W. Carlson, D.W. Curtis, G. Paschmann, W. Michel, Adv. Space Res. **2**, 67 (1982). https://doi.org/10.1016/0273-1177(82)90151-X

J.H. Clemmons, F.A. Herrero, Rev. Sci. Instrum. **69**, 2285 (1998). https://doi.org/10.1063/1.1148933

A.J. Coates, A.D. Johnstone, J.J. Sojka, G.L. Wrenn, Planet. Space Sci. **33**, 1267 (1985). https://doi.org/10.1016/0032-0633(85)90005-4

A.J. Coates, R.A. Frahm, D.R. Linder, D.O. Kataria, Y. Soobiah, G. Collinson, J.R. Sharber, J.D. Winningham, S.J. Jeffers, S. Barabash, J.A. Sauvaud, R. Lundin, M. Holmström, Y. Futaana, M. Yamauchi, A. Grigoriev, H. Andersson, H. Gunell, A. Fedorov, J.J. Thocaven, T.L. Zhang, W. Baumjohann, E. Kallio, H. Koskinen, J.U. Kozyra, M.W. Liemohn, Y. Ma, A. Galli, P. Wurz, P. Bochsler, D. Brain, E.C. Roelof, P. Brandt, N. Krupp, J. Woch, M. Fraenz, E. Dubinin, S. McKenna-Lawlor, S. Orsini, R. Cerulli-Irelli, A. Mura, A. Milillo, M. Maggi, C.C. Curtis, B.R. Sandel, K.C. Hsieh, K. Szego, A. Asamura, M. Grande, Planet. Space Sci. **56**, 802 (2008)

A.J. Coates, S.M.E. Tsang, A. Wellbrock, R.A. Frahm, J.D. Winningham, S. Barabash, R. Lundin, D.T. Young, F.J. Crary, Planet. Space Sci. **59**, 1019 (2011). https://doi.org/10.1016/j.pss.2010.07.016

G.A. Collinson, R. Frahm, A. Glocer, A.J. Coates, J.M. Grebowsky, S. Barabash, S.D. Domagal-Goldman, A. Fedorov, Y. Futaana, L.K. Gilbert, G. Khazanov, T.A. Nordheim, D. Mitchell, T.E. Moore, W.K. Peterson, J.D. Winningham, T.L. Zhang, Geophys. Res. Lett. (2016). https://doi.org/10.1002/2016GL068327

G.A. Collinson, L.B. Wilson, N. Omidi, D. Sibeck, J. Espley, C.M. Fowler, D. Mitchell, J. Grebowsky, C. Mazelle, S. Ruhunusiri, J. Halekas, R. Frahm, T. Zhang, Y. Futaana, B. Jakosky, J. Geophys. Res. Space Phys. **123**, 7241 (2018). https://doi.org/10.1029/2018JA025414

G.A. Collinson, A. Glocer, S. Xu, D. Mitchell, R.A. Frahm, J. Grebowsky, L. Andersson, B. Jakosky, Geophys. Res. Lett. **46**(3), 1168 (2019). https://doi.org/10.1029/2018GL080597

J.P. Doering, C.O. Bostrom, J.C. Armstrong, Radio Sci. **8**, 387 (1973). https://doi.org/10.1029/RS008i004p00387

J.P. Doering, W.K. Peterson, C.O. Bostrom, T.A. Potemra, Geophys. Res. Lett. **3**, 129 (1976). https://doi.org/10.1029/GL003i003p00129

C.L. Enloe, Rev. Sci. Instrum. **65**(2), 507 (1994). https://doi.org/10.1063/1.1145167

S.F. Fung, R.A. Hoffman, J. Geophys. Res. **96**, 3533 (1991). https://doi.org/10.1029/90JA02244

A. Glocer, T.I. Gombosi, G. Toth, K.C. Hansen, A.J. Ridley, A. Nagy, J. Geophys. Res. Space Phys. **112**, A01304 (2007). https://doi.org/10.1029/2006JA011755

A. Glocer, G. Tóth, T. Gombosi, D. Welling, J. Geophys. Res. Space Phys. **114**, A05216 (2009). https://doi.org/10.1029/2009JA014053

A. Glocer, N. Kitamura, G. Toth, T. Gombosi, J. Geophys. Res. Space Phys. **117**, A04318 (2012). https://doi.org/10.1029/2011JA017136

A. Glocer, G. Khazanov, M. Liemohn, J. Geophys. Res. Space Phys. **122**(6), 6708 (2017). https://doi.org/10.1002/2017JA024177

A. Glocer, G. Toth, M.C. Fok, J. Geophys. Res. Space Phys. **123**(4), 2851 (2018)

A. Glocer, D. Welling, C.R. Chappell, G. Toth, M.C. Fok, C. Komar, S.B. Kang, N. Buzulukova, C. Ferradas, S. Bingham, C. Mouikis, J. Geophys. Res. Space Phys. **125**(11), e28205 (2020). https://doi.org/10.1029/2020JA028205

G.V. Khazanov, M.W. Liemohn, T.E. Moore, J. Geophys. Res. **102**, 7509 (1997). https://doi.org/10.1029/96JA03343

M.W. Liemohn, G.V. Khazanov, T.E. Moore, S.M. Guiter, J. Geophys. Res. **102**, 7523 (1997). https://doi.org/10.1029/96JA03962

T.E. Moore, G.V. Khazanov, J. Geophys. Res. Space Phys. **115**(A14), A00J13 (2010). https://doi.org/10.1029/2009JA014905

T.E. Moore, C.R. Chappell, M.O. Chandler, P.D. Craven, B.L. Giles, C.J. Pollock, J.L. Burch, D.T. Young, J.H. Waite Jr., J.E. Nordholt, M.F. Thomsen, D.J. McComas, J.J. Berthelier, W.S. Williamson, R. Robson, F.S. Mozer, Science **277**, 349 (1997)

A.F. Nagy, P.M. Banks, J. Geophys. Res. **75**(31), 6260 (1970). https://doi.org/10.1029/JA075i031p06260

K.I. Oyama, C.H. Lee, H.K. Fang, C.Z. Cheng, Rev. Sci. Instrum. **83**(5), 055113 (2012). https://doi.org/10.1063/1.4722167

R.F. Pfaff, C. Steigies, M. Acuna, H. Freudenreich, T. Yeoman, S. Milan, M. Lester, P.E. Sandholt, K. Oksavik, J. Moen, J. Clemmons, P. Slocum, D. Knudsen, J. Burchill, M. Coplan, A. Gross, H. Deferaudy, L. Rezeau, D. Fontaine, J. Pincon, V. Krasnosselskikh, G. Delory, S. Basu, in *AGU Fall Meeting Abstracts, SM51D-01*, vol. 2003 (2003)

E. Shackleton, *South* (William Heinemann, London, 1919)

M.A. Shay, M. Swisdak, Phys. Rev. Lett. **93**(17), 175001 (2004). https://doi.org/10.1103/PhysRevLett.93.175001

S.C. Solomon, V.J. Abreu, J. Geophys. Res. Space Phys. **94**(A6), 6817 (1989). https://doi.org/10.1029/JA094iA06p06817

Y.J. Su, J.L. Horwitz, G.R. Wilson, P.G. Richards, D.G. Brown, C.W. Ho, J. Geophys. Res. **103**, 2279 (1998). https://doi.org/10.1029/97JA03085

H. Svedhem, D.V. Titov, D. McCoy, J.P. Lebreton, S. Barabash, J.L. Bertaux, P. Drossart, V. Formisano, B. Häusler, O. Korablev, W.J. Markiewicz, D. Nevejans, M. Pätzold, G. Piccioni, T.L. Zhang, F.W. Taylor, E. Lellouch, D. Koschny, O. Witasse, H. Eggel, M. Warhaut, A. Accomazzo, J. Rodriguez-Canabal, J. Fabrega, T. Schirmann, A. Clochet, M. Coradini, Planet. Space Sci. **55**, 1636 (2007)

E.P. Szuszczewicz, J. Appl. Phys. **43**, 874 (1972). https://doi.org/10.1063/1.1661297

C.C. Triplett, J. Li, R.L. Collins, G.A. Lehmacher, A. Barjatya, D.C. Fritts, B. Strelnikov, F.J. Lübken, B. Thurairajah, V.L. Harvey, D.L. Hampton, R.H. Varney, J. Geophys. Res., Atmos. **123**(23), 13,259 (2018). https://doi.org/10.1029/2018JD028788

R.H. Varney, S.C. Solomon, M.J. Nicolls, J. Geophys. Res. Space Phys. **119**, 8660 (2014). https://doi.org/10.1002/2013JA019378

D.T. Welling, V.K. Jordanova, S.G. Zaharia, A. Glocer, G. Toth, J. Geophys. Res. Space Phys. **116**(A2), A00J19 (2011). https://doi.org/10.1029/2010JA015642

J.D. Winningham, W.J. Heikkila, J. Geophys. Res. **79**(7), 949 (1974). https://doi.org/10.1029/JA079i007p00949

S. Xu, D. Mitchell, J. McFadden, G. Collinson, Y. Harada, R. Lillis, C. Mazelle, J. Connerney, Geophys. Res. Lett. (2018)

Authors and Affiliations

Glyn Collinson[1,2,3] · Alex Glocer[1] · Rob Pfaff[1] · Aroh Barjatya[4] · Scott Bissett[5] · Kolbjørn Blix[6] · Aaron Breneman[1] · Jim Clemmons[7] · Francis Eparvier[8] · Ted Gass[9] · Robert Michell[1] · David Mitchell[10] · Suzie Imber[11] · Ahmed Ghalib[12] · Hassanali Akbari[8] · Glen Ansted[12] · Lisa Baddeley[13] · Håvard Bahr[6] · Gary Bain[12] · Brian Bonsteel[12] · Henry Borgen[6] · Daniel Bowden[5] · Dave Bowker[12] · Tim Cameron[1] · Meredith Campbell[12] · Philip Cathell[12] · Dennis Chornay[1] · Robert Clayton[4] · Larry Conser[12] · Lance Davis[7] · Sean Donohue[12] · Leif Jonny Eilertsen[6] · Charles Etheridge[12] · Nathan Graves[4] · Ingemar Häggstrøm[14] · Preben Hanssen[6] · Herbert Haugh[12] · Espen Helgesen[15] · Jordan Henderson[12] · Kim Roar Herseth[6] · John Hickman[5] · Kent-Gøran Jensen[6] · Travis Jester[12] · Eric Johnson[12] · Hunter Johnson[12] · Andrew Kavanagh[16] · Max King[5] · David Knight[5] · Russell Laman[12] · Trevor Lankford[12] · Rolf Lien[6] · Mark Lester[11] · Gordon Marsh[5] · Steve Martin[1] · Norman Morris[12] · Long Nguyen[1] · Richard Nelson[12] · Wale Ogundere[5] · Karl Henning Osbakk[6] · Dave Page[12] · Joe Polidan[12] · Devon Raley[12] · Richard Raymond[12] · Ellen Robertson[1] · Giovanni Rosanova[12] · Traci Rosnack[1] · Belinda Serabian[12] · Roger Simonsen[6] · Jan Arne Søreng[6] · Jostein Sveen[6] · Diana Swanson[7] · Robert Swift[12] · Paulo Uribe[1] · Henry Valentine[4] · Frank Waters[12] · Libby West[5] · Tim Wilson[12]

✉ G. Collinson
glyn.a.collinson@nasa.gov

1 Heliophysics Science Division, NASA Goddard Space Flight Center, Greenbelt, MD, USA

2 The Catholic University of America, Washington, DC, USA

3 G&K Rocket Yards, Criccieth, Gwynedd, UK

4 Embry-Riddle Aeronautical University, Daytona Beach, FL, USA

5 NASA Sounding Rocket Program Office, NASA Wallops Flight Facility, Wallops Island, VA, USA

6 Andøya Space, Andenes, Norway

7 University of New Hampshire, Durham, NH, USA

8 Laboratory for Atmospheric and Space Physics, University of Colorado at Boulder, Boulder, CO, USA

9 NASA Wallops Flight Facility, Wallops Island, VA, USA

10 Space Science Laboratory, University of California at Berkeley, Berkeley, CA, USA

11 University of Leicester, Leicestershire, UK

12 NASA Sounding Rocket Operations Contract, NASA Wallops Flight Facility, Wallops Island, VA, USA

13 University Centre in Svalbard, Longyearbyen, Svalbard, Norway

14 EISCAT Headquarters, Kiruna, Sweden

15 The Arctic University of Norway, Longyearbyen, Svalbard, Norway

16 British Antarctic Survey, Cambridge, UK